Science and Technology Indonesia
e-ISSN:2580-4391 *p*-ISSN:2580-4405
Vol. 10, No. 4, October 2025

Research Paper

Temperature-Driven Optimization of $LiCoO_2$ Thin-Film Cathodes via Pulsed Laser Deposition: Structural and Morphological Control

Nur Ika Puji Ayu[1*], Abu Khalid Rivai[2,3], Evvy Kartini[4]

[1]*Department of Physics, Universitas Indonesia, Depok, 16424, Indonesia*
[2]*Research Organization for Nuclear Energy (ORTN), National Research and Innovation Agency (BRIN), Tangerang, 15314, Indonesia*
[3]*Research Center for Nuclear Beam Analysis Technology, National Research and Innovation Agency (BRIN), Tangerang, 15314, Indonesia*
[4]*Research Organization for Nanotechnology and Material (ORNM), National Research and Innovation Agency (BRIN), Tangerang, 15314, Indonesia*
***Corresponding author**: ayu.nip@sci.ui.ac.id

Abstract
Thin $LiCoO_2$ film cathodes were fabricated on a silicon substrate by Pulsed Laser Deposition (PLD). The microstructural properties were investigated as a function of the substrate temperature (T_s), which varied between 750°C, 850°C, and 900°C. The deposition was performed using a Nd:YAG laser (266 nm, 100 mJ) under an oxygen partial pressure of 200 mTorr. X-ray Diffraction (XRD) analysis revealed that films consist of HT-$LiCoO_2$ and a small amount of Co_3O_4 precipitates. The highest crystallinity was obtained for the thin film deposited at T_s = 900°C, whereas the Atomic Force Microscopy (AFM) indicated uniform grain size distributions of the film deposited at T_s = 850°C with an approximate surface roughness of 18 nm. The increase of surface roughness at higher T_s was attributed to non-uniform grain distribution, highlighting the importance of substrate temperature control in minimizing interfacial defects for improved electrochemical performance. This study provides key insights into the interplay between PLD parameters and film microstructure, offering a pathway for optimizing $LiCoO_2$ cathodes for thin-film batteries and advanced solid-state energy storage devices.

Keywords
Cathode, $LiCoO_2$ Thin Film, PLD, Substrate Temperature, Morphology

Received: 26 June 2025, Accepted: 28 August 2025
https://doi.org/10.26554/sti.2025.10.4.1215-1224

1. INTRODUCTION

Lithium-ion batteries (LIBs) have been in high demand worldwide for decades, since their broad application in portable electronics, electric vehicles, and renewable energy systems, due to their high energy density, long cycle life, and stable performance (Usai et al., 2022; Goodenough and Kim, 2010). The rise of the Internet of Things (IoT) (Chaudhary and Sharma, 2022; Zaheeruddin and Gupta, 2020), supported by the compactness of the modern electronic devices, including implants and wearable sensors, requires a durable power source. Thin film lithium-ion batteries (TFLIBs) are a promising candidate, which offers several advantages such as reduced thickness, low self-discharge, and flexibility (Xia et al., 2023). In addition, its solid-state architecture improves safety by removing the flammable liquid electrolyte, which is usually utilized in commercial lithium-ion batteries (Chen et al., 2021; Jaguemont and Bardé, 2023; Yu et al., 2023).

Nonetheless, TFLIBs as all-solid-state batteries (ASSBs) are challenged by several issues, such as interfacial stability, structural changes, residual stress, and cathode-electrolyte interface (CEI)(Maruno et al., 2025; Hirayama et al., 2021). Among these challenges, interfacial stability between the electrode and electrolyte is a critical factor affecting the performance and longevity of ASSBs (Yang et al., 2025; Lin and Lin, 2022). Such instability has been observed in various cathode materials, including $LiCoO_2$ (Ohnishi, 2024; Lu et al., 2017), $LiFePO_4$ (Moazzen et al., 2024; Dupre et al., 2018), and $LiMn_2O_4$ (Xia et al., 2025; Delluva et al., 2020). $LiCoO_2$, in particular, remains a widely studied cathode due to its high operating voltage (4.2 V vs Li/Li^+), specific energy capacity (69μAh/cm^2), long cycle life, and minimal self-discharge (Whittingham, 2004; Kawashima et al., 2020; Lyu et al., 2021). A few researchers have explored methods to improve interfacial stability in $LiCoO_2$ thin-film cathodes, particularly through post-deposition surface modifications such as coatings with graphene, Nd, or other oxide materials (Zhang et al., 2024; Hirayama et al., 2021; Chen et al., 2021; Lu et al., 2017). However, prior to coating, optimizing the initial microstructure, such as achieving low surface roughness, obtaining stable composition, and

improving film crystallinity, is crucial for enhancing ion transport and ensuring long-term cathode stability and performance (Nishio et al., 2016; Wu et al., 2022; Yang et al., 2025).

The microstructure and the crystallinity of the thin film cathodes depend on the preparation methods. $LiCoO_2$ thin film cathode can be prepared using various techniques, such as DC/RF and magnetron sputtering (Ganesh et al., 2018; Jung et al., 2013; Tintignac et al., 2014; Kurbatov et al., 2024; Ozcan et al., 2025), atmospheric plasma spraying (Hsueh et al., 2022), pulsed laser deposition (PLD) (Morozov et al., 2022; Yuan et al., 2022; Kwon et al., 2015), and sol–gel (Porthault et al., 2010) or hydrothermal methods (Porthault et al., 2016). Although $LiCoO_2$ is frequently prepared using DC/RF magnetron sputtering in liquid and solid electrolytes, these thin films frequently have low crystallinity and poor electrochemical efficiency. In contrast, laser-assisted synthesis routes have demonstrated precise control over oxide nano-structures, as shown in the case of calcium oxide nano-particles, where laser-induced plasma enabled tuning of crystallite size and surface morphology (Abbas and Aadim, 2022). Therefore, pulsed laser deposition (PLD) offers better control over film stoichiometry and promotes the formation of highly crystalline thin films (Fenech and Sharma, 2020), making it a promising technique for high-performance cathode fabrication.

There are two ways to improve the film crystallinity, ex-situ heat treatment after thin film formation or annealing process (Ta = 300°C up to 650°C) (Zhang et al., 2024; Kadhem, 2023), and in-situ annealing during deposition by heating the substrate (T_s = 600°C (Takeuchi et al., 2015). However, note that annealing processes post-deposition may induce lithium loss, interfacial stress due to heat expansion differences between substrate and film, or inhomogeneous grain formation. In contrast, in-situ crystallization during the PLD process promotes the formation of highly oriented and dense $LiCoO_2$ thin films and strengthens the film–substrate interface (Rao, 2010; Takeuchi et al., 2015). Thus, in the present study, we are concerned with in-situ heat treatment during the PLD process by controlling the substrate temperature (T_s). In addition, the intensive study of substrate temperature dependent on film morphology and crystallinity, to date, is lacking (Ohnishi and Takada, 2024). Substrate temperature during PLD plays a critical role in determining the crystallinity, surface morphology, and grain structure of $LiCoO_2$ films, which are closely linked to their electrochemical performance. Therefore, this study focuses on evaluating the effect of substrate temperature on the microstructural characteristics of $LiCoO_2$ thin films deposited on silicon substrates via PLD. The objective of this research is to identify the optimal deposition conditions to achieve high crystallinity, uniform grain size, and low surface roughness, thereby enhancing interfacial quality and contributing to the development of high-performance cathodes for solid-state thin-film lithium-ion batteries.

2. EXPERIMENTAL SECTION

2.1 Materials

$LiCoO_2$ films were grown on single crystal silicon (111) substrates (Nisicon, Japan). A sintered $LiCoO_2$ target pellet with 2,54 cm diameters was purchased from Praxair Surface Technologies, Inc.(USA). High-purity oxygen gas (99,999%) was used as the reactive atmosphere. Silver paste (Dotite, Japan) was used to bond the substrate to heater, ensuring effective thermal coupling during deposition.

2.2 Instruments

The $LiCoO_2$ thin films were deposited using a Pulsed Laser Deposition (PLD) system (Neocera Pioneer 120, USA) equipped with a Nd:YAG laser (λ = 266 nm) operating at 100 mJ and 5 ns pulsed. The microstructure and the chemical composition of the films were analyzed using a Scanning Electron Microscope equipped with Energy Dispersive X-ray (SEM-EDX, JEOL 6510 LA, Japan) operating at 20 keV and magnification up to ×20,000. The SEM images were captured from both the top view and the cross-section, and ImageJ software was employed to calculate the average grain size from the SEM image (Schneider et al., 2012). For further details of the microstructure evaluation, the surface morphology and root-mean-square (RMS) of the films were evaluated using an Atomic Force Microscope (AFM, Park Systems NX7, South Korea) operated in non-contact mode, and software XEI (Park Systems, South Korea) was used to estimate surface roughness with scans performed over a 10×10 μm^2 area at the rate of 0.1 Hz. The crystallinity and phase composition were characterized using an X-ray Diffractometer (Panalytical Empyrean, Netherlands) with Cu-Kα radiation at room temperature in a 2θ range of 15° to 90°, while complementary phase analysis was conducted using a Raman microscope (Bruker SENTERRA II, Germany) equipped with a 785 nm diode laser at 50 mW.

2.3 Procedures

The PLD chamber was initially evacuated to the base pressure of 1×10^{-5} Torr, followed by oxygen purging for approximately 30 min. The substrate with the size of about 15×10 mm was bonded to the heater surface with silver paste. The target-to-substrate distance was maintained at 5 cm. The deposition was carried out under an oxygen partial pressure of 200 mTorr at a laser repetition rate of 10 Hz for 120 min. The silicon substrate temperature was varied by setting the heater to 750°C, 850°C, and 900°C. The deposition was performed under an oxygen partial pressure of 200 mTorr for 120 min and a repetition rate of 10 Hz. To mitigate stress accumulation and prevent localized target erosion, the target was continuously rotated during deposition. After deposition, the films were cooled to room temperature at a rate of 10°C/s and subsequently purged with nitrogen.

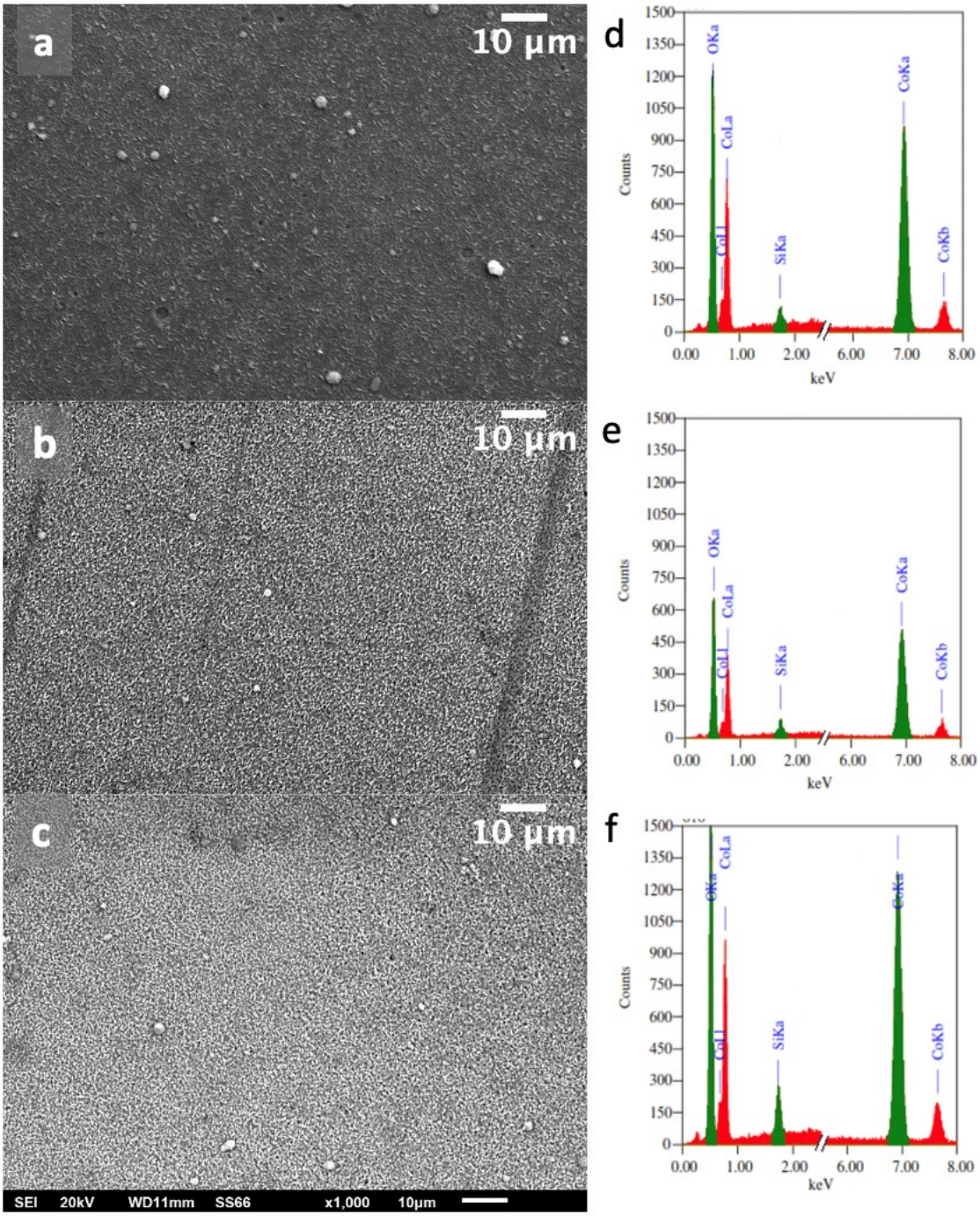

Figure 1. SEM and EDX of of the $LiCoO_2$ Thin Film Surface on 1000× Magnification for the Sample Deposited at (a,d) 750°C, (b,e) 850°C, and (c,f) 900°C

3. RESULTS AND DISCUSSION

As demonstrated by Morozov et al. (2022) and Rao (2010), the micro-structural properties of thin-film cathodes critically affect their electrochemical performance. This study systematically explores the influence of substrate temperature on the microstructure and crystallinity of $LiCoO_2$ thin films, which in turn affects their functional performance.

Figure 1(a)-(c) shows the SEM image of the $LiCoO_2$ after deposition, which revealed uniform grain sizes with high packing density across all deposited film. The films deposited at T_s = 750°C shows prominently larger white granules relatives to the other samples. EDX mapping (Figure 1(d)-(f))

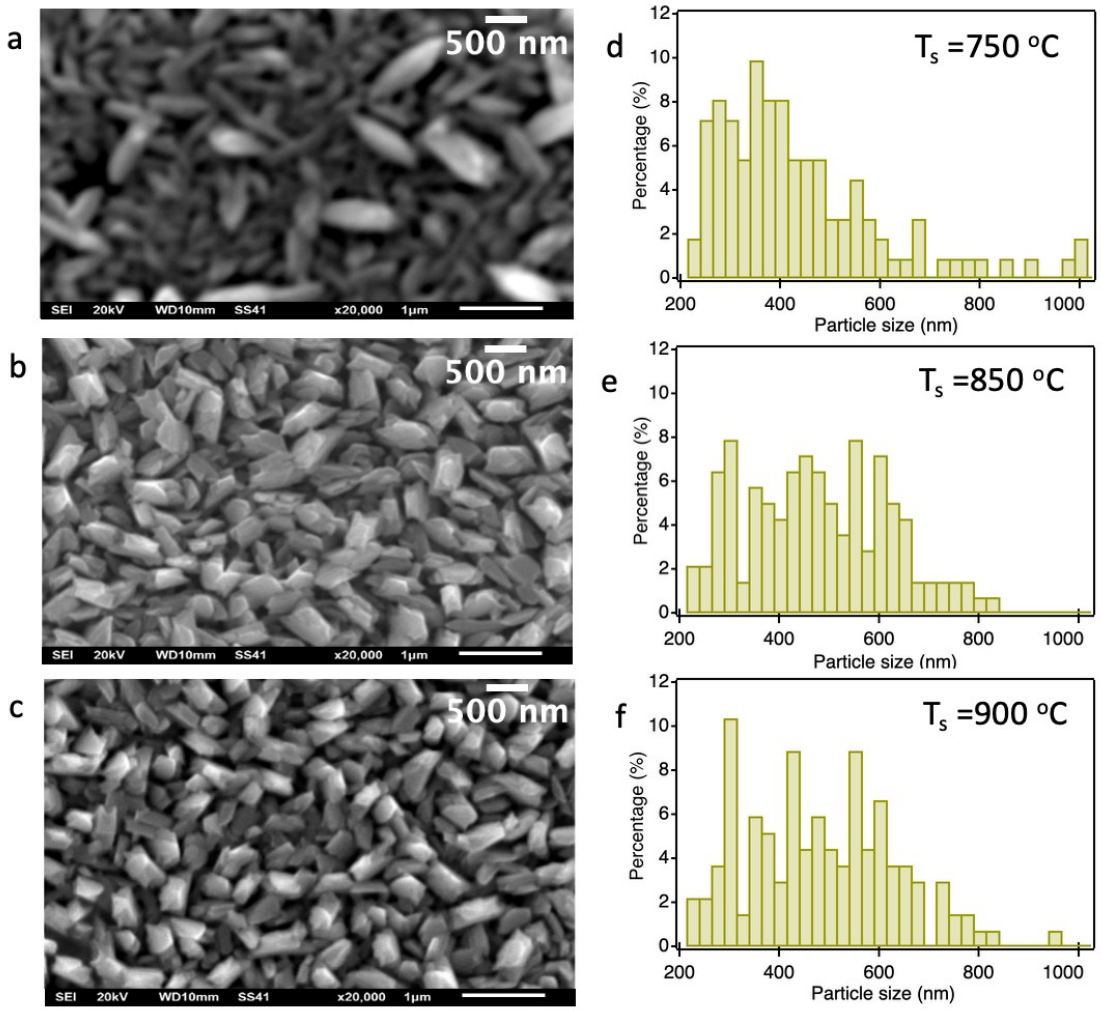

Figure 2. SEM Images (20,000×) and Particle Size Distributions of $LiCoO_2$ Thin Films Deposited at (a,d) 750°C, (b,e) 850°C, and (c,f) 900°C, with Particles Size Estimated Using ImageJ Software (Schneider et al., 2012)

Table 1. Average Grain Size of $LicoO_2$ Thin Films Calculated from SEM Images (Figure 2: A-C) Using Imagej Software (Schneider et al., 2012)

Deposition Parameters of T_s (°C)	Mean (nm)	Min (nm)	Max (nm)	Standard deviation (σ)
750	429	207	1050	180
850	461	202	820	143
900	468	201	945	151

confirmed the predominant composition of the $LiCoO_2$ phase. However, sporadic granular features were observed distributed randomly on the surface. These secondary phases were identified as Co_3O_4, consistent with previous reports by Rao (2010) on PLD-grown $LiCoO_2$ films and observation by Azib et al. (2015) in hydrothermally synthesized films. The formation of Co_3O_4 indicates partial oxidation of Co in $LiCoO_2$ during deposition, which may be triggered by local oxygen excess at the substrate interface, slight pressure fluctuations during the process, and kinetic competition between the nucleation of $LiCoO_2$ and Co_3O_4 phases.

Figure 2 shows SEM images at a higher magnification of 20,000× and particle size distribution of $LiCoO_2$, indicating a clear trend of grain refinement with increasing substrate temperature. The particle size distribution of the $LiCoO_2$ films was estimated using ImageJ software and the results are summarized in Table 1. At T_s = 750°C, the film exhibits a broad distribution, with grain sizes extending from 207 nm up to approximately 1050 nm. The films deposited at 850°C and 900°C show closely similar average particle sizes of 461 and

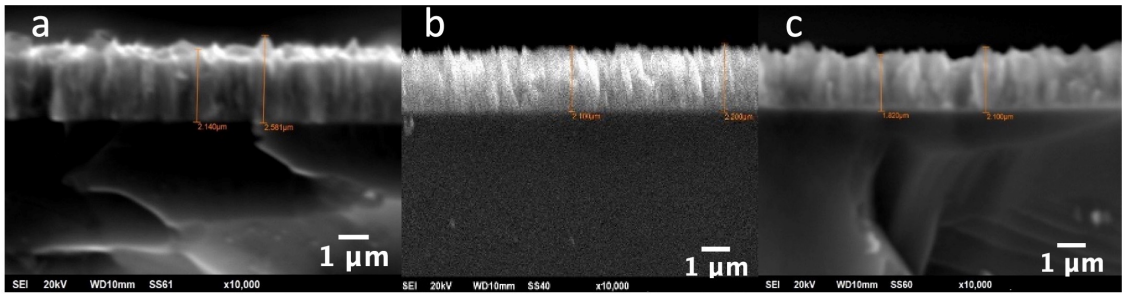

Figure 3. SEM Cross Section of the $LiCoO_2$ Thin Film Deposited at (a) 750°C, (b) 850°C, and (c) 900°C

Table 2. Deposition Parameters of $LiCoO_2$ Film

Parameters	This work	(Rao, 2010)	(Perkins et al., 2001)	(Maruyama et al., 2016)	(Takeuchi et al., 2015)	(Matsuda et al., 2018)
Laser source	Nd:YAG	KrF	KrF	KrF	KrF	ArF
Laser λ (nm)	266	248	248	248	248	193
O_2 pressure (mTorr)	200	100	2000	200	200	150
TS (°C)	750, 850, 900	300	700	550	600	600
Roughness (nm)	22, 18, 28	18	100 (grain)	0.84	2 (grooves)	66-80 (grain)
Substrate	Si	Si	SnO_2	$SrTiO_3$	$SrTiO_3$	$Pt/Cr/SiO_2$

468 nm, respectively, indicating well-controlled growth conditions. At 850°C, the distribution narrows and centers around 400–600 nm, representing more uniform grain and improved film homogeneity. At 900°C, the distribution back toward smaller sizes with broader tail up to 900 nm, which may due to grain nucleation and competition. These results suggest that a deposition temperature of 850°C yields the most uniform particle size distribution with lowest standard deviation of particle size distributions. Compared to the grain sizes reported by Perkins (100 nm) (Perkins et al., 2001) , our results were larger, which may be attributed to the higher deposition temperatures promoting grain growth.

Figure 3 shows cross-sectional SEM images of $LiCoO_2$ films, revealing a transition from columnar to more equiaxed grains with increasing temperature. At 850°C, the films become denser with a refined columnar structure, indicating enhanced surface diffusion and grain growth. At 900°C, significant grain coarsening is observed, likely driven by thermal stress. These observations are consistent with previous studies on temperature-dependent micro-structural evolution in oxide films (Nishio et al., 2016), where elevated substrate temperatures typically enhance densification but lead to the formation of mechanical defects. From these clear contrast images and reliable differentiation between the film and substrate, we observed uniform film thickness for all samples (2μm), reflecting a consistent deposition rate of 16 nm/min, independent of the substrate temperature. This temperature-independent thickness behavior aligns with Nishio et al. (2016), suggesting that substrate temperature primarily influences surface crystallization processes rather than deposition kinetics. These results demonstrate that while temperature significantly modifies film morphology, it has minimal impact on deposition rates and film thickness.

Figure 4 shows AFM topography revealing homogeneous grain distribution and a clear temperature-dependent evolution in surface morphology. The quantitative analysis was performed on XEI software. Film grown at 750°C exhibited columnar grains with a relatively broad grain size distribution (909 nm average) and surface roughness (22 nm) due to incomplete grain coalescence. In contrast, films deposited at 850°C showed a more uniform, dense microstructure with equiaxed grains (723 nm average) and the lowest surface roughness (18 nm), indicating optimal growth conditions that balanced nucleation and surface diffusion rates. Although higher temperatures (900°C) typically promote grain growth, the observed surface roughness (28 nm) suggests competing mechanisms, where extended thermalization enables both particle coalescence and nonuniform surface diffusion, resulting in irregular grain structures. Table 2 summarizes the deposition parameters adopted in the previous study. The lowest roughness was obtained by Maruyama et al. (2016) combinatorial synthesis from the Li_2CO_3 and CoO annealing that required the simultaneous control of multiple parameters and was challenging to implement. In contrast, the direct deposition as adopted in our study is more feasible. Our results aligns closely with Rao (2010), with addition to the higher deposition temperature to achieve higher film crystallinity.

Figure 5 (a) shows the XRD pattern of the films, confirming the predominant formation of high- temperature phase $LiCoO_2$ (HT-$LiCoO_2$ space group R -3m), especially in the film grown at 850 and 900°C. At 750°C, the diffraction peak of $LiCoO_2$ could not be distinguished, which may indicate the

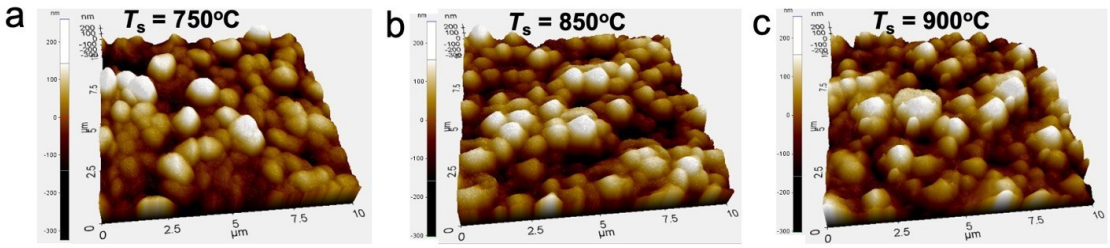

Figure 4. AFM Topography of $LiCoO_2$ Thin Film Deposited at (a) 750°C, (b) 850°C, and (c) 900°

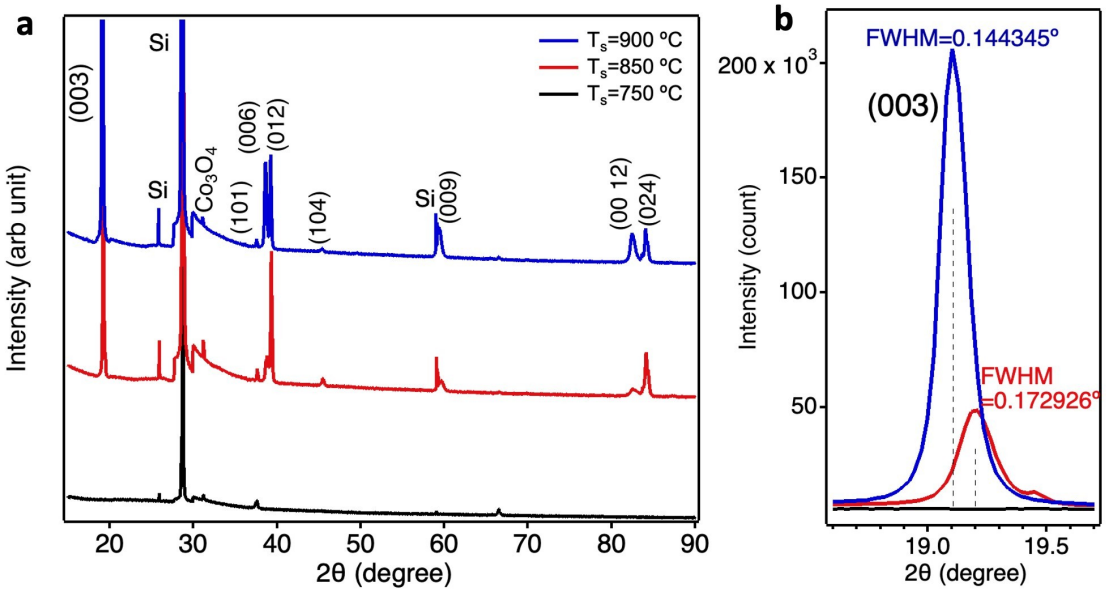

Figure 5. (a) X-Ray Diffraction (XRD) Pattern of the $LiCoO_2$ Thin Films and (b) the Magnification of the (003)-peak

amorphous phase. A minor Co_3O_4 phase (less than 5 wt%) was detected, indicating partial segregation likely due to lithium deficiency or local oxygen excess, consistent with SEMEDX results and prior reports (Rao, 2010; Yamada et al., 2013). Crystal structure of $LiCoO_2$ thin film affects its electrochemical performance (Jung et al., 2013; Yamada et al., 2013; Xia and Lu, 2007), where the high-temperature phase (HT-$LiCoO_2$, *R* -3m) shows better performance than the low-temperature cubic phase (LT-$LiCoO_2$, *Fd* -3m), attributed to enhanced two-dimensional conductivity of lithium-ion. The clear identification of HT-$LiCoO_2$ confirms the effectiveness of our deposition temperatures in stabilizing the electrochemically active layered structure.

The dominant peak of (003) around 2θ = 18.9° indicates preferential crystallographic orientation along the layered planes, which is a favorable configuration for lithium-ion intercalation. Figure 5(b) shows the XRD (003) reflection of the films. The absence of this peak at 750°C indicates an amorphous structure, suggesting crystallization occurs above this temperature. Previous studies have shown that deposition at 300°C or lower typically yields poorly crystalline or amorphous films, whereas higher substrate temperatures result in films with sufficiently good crystallinity (Ohnishi et al., 2015). The HT-$LiCoO_2$ is also known to be stable at relatively high temperatures around 800°C, through thermal synthesis (Pegoretti et al., 2017). Therefore, annealing thin film above 700°C has been reported to promote the formation of the high-temperature phase, which is essential for maintaining structural integrity during battery cycling (Donders et al., 2013; Ohnishi, 2024). Increasing the substrate temperature to 900°C significantly enhances crystallinity, as evidenced by the narrowing full-width half maximum (FWHM) of the (003)-peak. Improved crystal quality is expected to reduce charge transfer resistance by minimizing defects and lithium pathway disorder (Xia and Lu, 2007). PLD-grown $LiCoO_2$ films typically exhibit (00l) orientation due to their low formation energy and favorable vertical growth kinetics, though substrate orientation may also play a role (Kwon et al., 2015). Films with (003) orientation have shown superior electrochemical performance compared to those with (104) orientation (Xia and Lu, 2007; Qiu et al., 2025). However, at 900°C, increased roughness (28 nm) may offset the benefits of enhanced crystallinity.

While substrate orientation strongly influences film texture (Ohnishi et al., 2021; Kwon et al., 2015; Xia et al., 2006),

our 2 μm-thick $LiCoO_2$ films predominantly exhibit (003) orientation, deviating from theoretical expectations favoring (101)/(104) textures to relieve strain (Xia and Lu, 2007; Bates et al., 2000). This aligns with Jung's findings (Jung et al., 2013), suggesting that PLD growth is governed by competing factors, such as the low surface energy of (003) facets and dynamic strain accommodation via grain boundary formation. The performance differences reported across (003)-oriented films (Kwon et al., 2015) versus advantages in randomly oriented (Tang et al., 2006) or (104)-textured films (Ohnishi et al., 2021; Ohnishi and Takada, 2024; Ozcan et al., 2025) may be reconciled by the coexistence of through-plane diffusion (dominant in (003)) and grain-boundary-assisted transport in polycrystalline films. In our system, the presence of dominant (003) orientation with minor secondary textures may strike a balance between these pathways. Moreover, the 2 μm film thickness provides sufficient material to sustain capacity without inducing excessive strain. These XRD results are consistent with AFM observations of grain size heterogeneity, highlighting how elevated temperatures enhance crystallinity while introducing micro-structural disorder through competitive grain growth and non-uniform strain. This interplay presents a key optimization challenge, while larger crystallites can enhance ionic conductivity, associated strain and grain size variation may compromise mechanical stability during cycling.

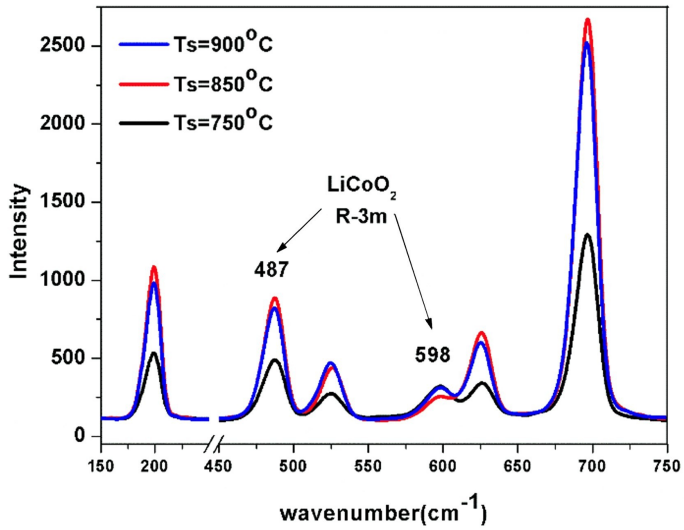

Figure 6. Raman Spectra of the $LiCoO_2$ Thin Films Deposited at (a) 750°C, (b) 850°C, and (c) 900°C

Figure 6 presents Raman spectra of the $LiCoO_2$ films, which identify characteristic vibrational modes of the main phase $LiCoO_2$. The presence of secondary phase Co_3O_4 was also observed at 674 cm^{-1} in agreement with SEM-EDX and XRD results. The vibrational modes of rhombohedral $LiCoO_2$ primarily reflect oxygen sub-lattice vibration, which correspond to the E_g bending mode (487 cm^{-1}) and A_{1g} stretching mode (598 cm^{-1}), in agreement with previous reports (Otoyama et al., 2016; Matsuda et al., 2019). The E_g mode (487 cm^{-1}) corresponds to O−Co−O bending vibrations, and the A_{1g} mode (598 cm^{-1}) represents Co−O symmetric stretching. As quantified in Table 3, the relative intensity ratio (A_{1g}/E_g) was maximum for films deposited at 850°C, suggesting enhanced c-axis orientation at this temperature. This trend correlates with XRD-determined (003)-peak intensity variations.

Table 3. Intensity Ratio of E_g/A_{1g} Vibrational Modes from Raman Spectrum

Deposition Parameters T_s (°C)	E_g	A_{1g}	E_g/A_{1g}
750	378.322	191.813	1.972
850	774.346	145.001	5.340
900	711.176	192.108	3.702

The orientation dependence arises because the A1g mode intensity is maximized when the Co−O bond vectors align perpendicular to the substrate, while the Eg mode remains relatively insensitive to orientation. Films grown at 850°C demonstrate optimal crystallographic alignment (E_g/A_{1g} ratio 2.1 vs 1.7 at 750°C), reduced lattice disorder (FWHM of A_{1g} mode 18 cm^{-1} vs. 24 cm^{-1} at 900°C), and minimal secondary phase content (Co_3O_4 peak intensity less than 5% of A_{1g}). These structural advantages explain the superior electrochemical behavior of 850°C-grown films, where aligned Li^+ diffusion channels and reduced grain boundary resistance enhance performance.

4. CONCLUSIONS

$LiCoO_2$ thin film cathodes were successfully fabricated via pulsed laser deposition (PLD) using a Nd:YAG laser (λ = 266 nm). Structural analysis confirmed the formation of the high-temperature rhombohedral phase ($R\bar{3}m$) with minimal Co_3O_4 impurity (< 5%), attributed to lithium deficiency during deposition. A systematic investigation of substrate temperature revealed that 850 °C yields the most favorable balance between crystallinity and surface morphology. At this temperature, films exhibited strong (003) orientation, minimal surface roughness (18 nm), and intermediate grain size (100 nm), supporting efficient Li-ion transport through both bulk and grain boundaries. In contrast, lower temperatures (750 °C) resulted in poor crystallinity and high porosity, while higher temperatures (900 °C) led to excessive grain coarsening and roughness (above 28 nm), potentially compromising interfacial stability. The superior phase and orientation at 850 °C, corroborated by Raman analysis, highlight its suitability for fabricating high-performance cathodes, particularly for all-solid-state microbatteries where smooth interfaces and controlled thickness are critical. These findings provide a framework for optimizing PLD conditions in $LiCoO_2$-based electrodes. The electrochemical validation, including cycling stability and rate capability, may be needed to fully assess their application potential in advanced Li-ion systems for future work.

5. ACKNOWLEDGMENT

The authors would like to thank the Ministry of Research, Technology, and Higher Education of the Republic of Indonesia (Kemristekdikti RI) for the research funding on thin-film battery development at the National Research and Innovation Agency (BRIN). We also extend our appreciation to colleagues at the Research Center for Advanced Materials for their technical assistance and access to PLD facilities.

REFERENCES

Abbas, I. K. and K. A. Aadim (2022). Synthesis and Study of Structural Properties of Calcium Oxide Nanoparticles Produced by Laser-Induced Plasma and Its Effect on Antibacterial Activity. *Science and Technology Indonesia*, **7**(4); 427–434

Azib, T., F. Le Cras, and H. Porthault (2015). Direct Fabrication of $LiCoO_2$ Thin-Films in Water–Ethanol Solutions by Electrochemical–Hydrothermal Method. *Electrochimica Acta*, **160**; 145–151

Bates, J. B., N. J. Dudney, B. J. Neudecker, F. X. Hart, H. P. Jun, and S. A. Hackney (2000). Preferred Orientation of Polycrystalline $LiCoO_2$ Films. *Journal of The Electrochemical Society*, **147**(1); 59

Chaudhary, D. and P. C. Sharma (2022). An Overview of Internet of Things Related Protocols, Technologies, Challenges and Application. In *Ambient Intelligence and Internet of Things*. John Wiley & Sons, Ltd, pages 33–52

Chen, Y., Y. Kang, Y. Zhao, L. Wang, J. Liu, Y. Li, and B. Li (2021). A Review of Lithium-Ion Battery Safety Concerns: The Issues, Strategies, and Testing Standards. *Journal of Energy Chemistry*, **59**; 83–99

Delluva, A. A., J. Dudoff, G. Teeter, and A. Holewinski (2020). Cathode Interface Compatibility of Amorphous $LiMn_2O_4$ (LMO) and $Li_7La_3Zr_2O_{12}$ (LLZO) Characterized With Thin-Film Solid-State Electrochemical Cells. *ACS Applied Materials & Interfaces*, **12**(22); 24992–24999

Donders, M. E., W. M. Arnoldbik, H. C. M. Knoops, W. M. M. Kessels, and P. H. L. Notten (2013). Atomic Layer Deposition of $LiCoO_2$ Thin-Film Electrodes for All-Solid-State Li-Ion Microbatteries. *Journal of The Electrochemical Society*, **160**(5); A3066

Dupre, N., M. Cuisinier, Y. Zheng, V. Fernandez, J. Hamon, M. Hirayama, and D. Guyomard (2018). Evolution of $LiFePO_4$ Thin Films Interphase With Electrolyte. *Journal of Power Sources*, **382**; 45–55

Fenech, M. and N. Sharma (2020). Pulsed Laser Deposition-Based Thin Film Microbatteries. *Chemistry – An Asian Journal*, **15**(12); 1829–1847

Ganesh, K. S., B. P. Reddy, P. J. Kumar, and O. Hussain (2018). Influence of Zr Dopant on Microstructural and Electrochemical Properties of $LiCoO_2$ Thin Film Cathodes by RF Sputtering. *Journal of Electroanalytical Chemistry*, **828**; 71–79

Goodenough, J. B. and Y. Kim (2010). Challenges for Rechargeable Li Batteries. *Chemistry of Materials*, **22**(3); 587–603

Hirayama, M., K. Suzuki, R. Kanno, T. Masuda, and K. Tamura (2021). Characterization of Cathode/Sulfide Electrolyte Interface Using a Thin-Film Model Battery. In K. Kanamura, editor, *Next Generation Batteries: Realization of High Energy Density Rechargeable Batteries*. Springer Singapore, Singapore, pages 167–178

Hsueh, T.-H., C.-H. Tsai, S.-E. Liu, M.-C. Wang, S.-M. Chang, A. Shiue, and K.-Y. Chin (2022). $LiCoO_2$ Battery Electrode Fabricated by High Deposition-Rate Atmospheric Plasma Spraying for Lithium Battery. *Journal of The Electrochemical Society*, **169**(10); 100506

Jaguemont, J. and F. Bardé (2023). A Critical Review of Lithium-Ion Battery Safety Testing and Standards. *Applied Thermal Engineering*, **231**; 121014

Jung, K.-T., G.-B. Cho, K.-W. Kim, T.-H. Nam, H.-M. Jeong, S.-C. Huh, and J.-P. Noh (2013). Influence of the Substrate Texture on the Structural and Electrochemical Properties of Sputtered LiCoO2 Thin Films. *Thin Solid Films*, **546**; 414–417. The Proceedings of International Union of The Materials Research Society - International Conference in Asia 2012 (IUMRS-ICA 2012)

Kadhem, S. J. (2023). Preparation of Al_2O_3/PVA Nanocomposite Thin Films by a Plasma Jet Method. *Science and Technology Indonesia*, **8**(3); 471–478

Kawashima, K., T. Ohnishi, and K. Takada (2020). High-Rate Capability of $LiCoO_2$ Cathodes. *ACS Applied Energy Materials*, **3**(12); 11803–11810

Kurbatov, S. V., A. S. Rudy, V. V. Naumov, A. A. Mironenko, O. V. Savenko, M. A. Smirnova, and D. E. Pukhov (2024). A Comprehensive Study of Nonuniformity Properties of The $LiCoO_2$ Thin-Film Cathode Fabricated by RF Sputtering. *Russian Microelectronics*, **53**(3); 202–216

Kwon, T., T. Ohnishi, K. Mitsuishi, T. C. Ozawa, and K. Takada (2015). Synthesis of $LiCoO_2$ Epitaxial Thin Films Using a Sol–Gel Method. *Journal of Power Sources*, **274**; 417–423

Lin, C. and S. Lin (2022). Issues, Developments, and Computation Analyses of Interfacial Stability in All-Solid-State Li Batteries. *JOM*, **74**(12); 4654–4663

Lu, W., J. Zhang, J. Xu, X. Wu, and L. Chen (2017). In Situ Visualized Cathode Electrolyte Interphase on $LiCoO_2$ in High Voltage Cycling. *ACS Applied Materials & Interfaces*, **9**(22); 19313–19318

Lyu, Y., X. Wu, K. Wang, Z. Feng, T. Cheng, Y. Liu, and B. Guo (2021). An Overview on The Advances of $LiCoO_2$ Cathodes for Lithium-Ion Batteries. *Advanced Energy Materials*, **11**(2); 2000982

Maruno, M., F. Nakayama, Y. Suzuki, M. Sakakura, T. Ohnishi, Y. Nomura, and Y. Iriyama (2025). Chemical Design Rules for Low-Resistivity Electrode–Electrolyte Interfaces in All-Solid-State Lithium Batteries. *Communications Materials*, **6**(1); 144

Maruyama, S., O. Kubokawa, K. Nanbu, K. Fujimoto, and

Y. Matsumoto (2016). Combinatorial Synthesis of Epitaxial $LiCoO_2$ Thin Films on $SrTiO_3$(001) Via On-Substrate Sintering of Li_2CO_3 and CoO by Pulsed Laser Deposition. *ACS Combinatorial Science*, **18**(6); 343–348

Matsuda, Y., N. Kuwata, and J. Kawamura (2018). Thin-Film Lithium Batteries With 0.3–30 um Thick LiCoO2 Films Fabricated by High-Rate Pulsed Laser Deposition. *Solid State Ionics*, **320**; 38–44

Matsuda, Y., N. Kuwata, T. Okawa, A. Dorai, O. Kamishima, and J. Kawamura (2019). In Situ Raman Spectroscopy of $LixCoO_2$ Cathode in $Li/Li_3PO_4/LiCoO_2$ All-Solid-State Thin-Film Lithium Battery. *Solid State Ionics*, **335**; 7–14

Moazzen, E., J. Mujtaba, B. Buchholz, D. Isheim, N. S. Luu, D. Rowell, and S. A. Barnett (2024). Atom Probe Tomography of the $LiFePO_4$-Electrolyte Interface Enabled by Thin Film Electrodes. *Journal of The Electrochemical Society*, **171**(7); 070527

Morozov, A. V., H. Paik, A. O. Boev, D. A. Aksyonov, S. A. Lipovskikh, K. J. Stevenson, and A. M. Abakumov (2022). Thermodynamics As a Driving Factor of $LiCoO_2$ Grain Growth on Nanocrystalline Ta-LLZO Thin Films for All-Solid-State Batteries. *ACS Applied Materials & Interfaces*, **14**(35); 39907–39916

Nishio, K., T. Ohnishi, M. Osada, N. Ohta, K. Watanabe, and K. Takada (2016). Influences of High Deposition Rate on $LiCoO_2$ Epitaxial Films Prepared by Pulsed Laser Deposition. *Solid State Ionics*, **285**; 91–95. The 40th Symposium on Solid State Ionics in Japan

Ohnishi, T. (2024). Fabrication of Thin-Film Batteries Composed of $LiCoO_2$,Li_3PO_4, and Li Layers. *Journal of Solid State Electrochemistry*, **28**(12); 4355–4366

Ohnishi, T., K. Mitsuishi, and K. Takada (2021). In Situ X-Ray Diffraction of $LiCoO_2$ in Thin-Film Batteries Under High-Voltage Charging. *ACS Applied Energy Materials*, **4**(12); 14372–14379

Ohnishi, T., K. Nishio, and K. Takada (2015). Composition Controlled $LiCoO_2$ Epitaxial Thin Film Growth by Pulsed Laser Deposition. In F. H. Teherani, D. C. Look, and D. J. Rogers, editors, *Oxide-Based Materials and Devices VI*, volume 9364. SPIE, page 93640L

Ohnishi, T. and K. Takada (2024). Thin Film Battery With Epitaxial $LiCoO_2$ Cathode. In Y. Iriyama, K. Amezawa, Y. Tateyama, and N. Yabuuchi, editors, *Interface Ionics: For All-Solid-State Batteries and Solid State Ionics Devices*. Springer Nature Singapore, Singapore, pages 21–31

Otoyama, M., Y. Ito, A. Hayashi, and M. Tatsumisago (2016). Raman Imaging for $LiCoO_2$ Composite Positive Electrodes in All-Solid-State Lithium Batteries Using Li_2S–P_2S_5 Solid Electrolytes. *Journal of Power Sources*, **302**; 419–425

Ozcan, P., N. Esen, A. Cantas, L. Ozyuzer, M. Ozdemir, K. Kosiel, and G. Aygun (2025). Investigation of $LiCoO_2$ Thin Films Grown Under Relatively Low Substrate Temperature for All Solid State Lithium Ion Battery Applications. *Vacuum*, **239**; 114439

Pegoretti, V., P. Dixini, P. Smecellato, S. Biaggio, and M. Freitas (2017). Thermal Synthesis, Characterization and Electrochemical Study of High-Temperature (HT) $LiCoO_2$ Obtained from $Co(OH)_2$ Recycled of Spent Lithium Ion Batteries. *Materials Research Bulletin*, **86**; 5–9

Perkins, J. D., C. S. Bahn, J. M. McGraw, P. A. Parilla, and D. S. Ginley (2001). Pulsed Laser Deposition and Characterization of Crystalline Lithium Cobalt Dioxide ($LiCoO_2$) Thin Films. *Journal of The Electrochemical Society*, **148**(12); A1302

Porthault, H., F. Le Cras, J.-M. Duffault, and S. Franger (2016). Fast Deposition of Conformal $LiCoO_2$ Thin Film Electrodes for High Capacity 3D Batteries. *Materials Science and Engineering: B*, **213**; 163–168

Porthault, H., F. Le Cras, and S. Franger (2010). Synthesis of $LiCoO_2$ Thin Films by Sol/Gel Process. *Journal of Power Sources*, **195**(19); 6262–6267

Qiu, J., H. Li, T. Wu, Y. He, R. Xu, Y. Hua, and Y. Cui (2025). Construction of Longitudinal (003) Textured Low-Strain Diffusion Channel in 4.6 V $LiCoO_2$-Based All-Solid-State Thin Film Battery for Microelectronic Systems. *ACS Energy Letters*, **20**(7); 3249–3258

Rao, M. (2010). Growth and Microstructural Features of Laser Ablated $LiCoO_2$ Thin Films. *Journal of Crystal Growth*, **312**(19); 2799–2803

Schneider, C. A., W. S. Rasband, and K. W. Eliceiri (2012). NIH Image to ImageJ: 25 Years of Image Analysis. *Nature Methods*, **9**(7); 671–675

Takeuchi, S., H. Tan, K. K. Bharathi, G. R. Stafford, J. Shin, S. Yasui, and L. A. Bendersky (2015). Epitaxial $LiCoO_2$ Films as a Model System for Fundamental Electrochemical Studies of Positive Electrodes. *ACS Applied Materials & Interfaces*, **7**(15); 7901–7911

Tang, S., M. Lai, and L. Lu (2006). Effects of Oxygen Pressure on $LiCoO_2$ Thin Film Cathodes and Their Electrochemical Properties Grown by Pulsed Laser Deposition. *Journal of Alloys and Compounds*, **424**(1); 342–346

Tintignac, S., R. Baddour-Hadjean, J. Pereira-Ramos, and R. Salot (2014). High Rate Bias Sputtered $LiCoO_2$ Thin Films as Positive Electrode for All-Solid-State Lithium Microbatteries. *Electrochimica Acta*, **146**; 472–476

Usai, L., J. J. Lamb, E. Hertwich, O. S. Burheim, and A. H. Strømman (2022). Analysis of the Li-Ion Battery Industry in Light of the Global Transition to Electric Passenger Light Duty Vehicles Until 2050. *Environmental Research: Infrastructure and Sustainability*, **2**(1); 011002

Whittingham, M. S. (2004). Lithium Batteries and Cathode Materials. *Chemical Reviews*, **104**(10); 4271–4302

Wu, T., Y. Zhao, X. Zhang, S. Ma, K. Wei, Y. Wei, and Y. Cui (2022). Improved Solid Interfacial Kinetics and Electrochemical Performance for $LiCoO_2$(110) Textured Thin-Film Lithium Batteries. *Applied Surface Science*, **591**; 153174

Xia, H. and L. Lu (2007). Texture Effect on the Electrochemical Properties of $LiCoO_2$ Thin Films Prepared by PLD. *Electrochimica Acta*, **52**(24); 7014–7021

Xia, H., L. Lu, and G. Ceder (2006). Substrate Effect on the

Microstructure and Electrochemical Properties of $LiCoO_2$ Thin Films Grown by PLD. *Journal of Alloys and Compounds*, **417**(1-2); 304–310

Xia, Q., X. Lei, F. Yue, W. Liu, C. Xu, J. Xu, and H. Xia (2025). Unraveling the LiMn2O4/LiPON Interface Degradation in All-Solid-State Thin-Film Lithium Batteries. *Nano Letters*, **25**(19); 7892–7899

Xia, Q., F. Zan, Q. Zhang, W. Liu, Q. Li, Y. He, and H. Xia (2023). All-Solid-State Thin Film Lithium/Lithium-Ion Microbatteries for Powering the Internet of Things. *Advanced Materials*, **35**(2); 2200538

Yamada, H., T. S. Suzuki, T. Uchikoshi, M. Hozumi, T. Saito, and Y. Sakka (2013). Ideal Design of Textured $LiCoO_2$ Sintered Electrode for Li-Ion Secondary Battery. *APL Materials*, **1**(4); 042110

Yang, L., W. Wang, L. Wang, H. Zhang, D. Zhang, N. Sharma, and J. Seidel (2025). Nanoscale Ion Diffusion and Electric Charging–Discharging in Oriented Textured $LiCoO_2$ Thin Films. *ACS Applied Electronic Materials*, **7**(8); 3536–3542

Yu, X., R. Chen, L. Gan, H. Li, and L. Chen (2023). Battery Safety: From Lithium-Ion to Solid-State Batteries. *Engineering*, **21**; 9–14

Yuan, K., M. Xie, W. Dong, P. Zhao, J. Pan, Z. Liu, and F. Huang (2022). High-Speed and One-Step Deposition of a $LiCoO_2$ Thin-Film Electrode by a High-Repetition 1064 Nm Nd:YAG Fiber Laser. *ACS Applied Energy Materials*, **5**(12); 15483–15490

Zaheeruddin and H. Gupta (2020). Foundation of IoT: An Overview. In M. Alam, K. A. Shakil, and S. Khan, editors, *Internet of Things IoT: Concepts and Applications*. Springer International Publishing, Cham, pages 3–24

Zhang, C., J. Lou, J. Li, J. Song, Z. Qi, S. Huo, and L. Liu (2024). Graphene Coating-Modified $LiCoO_2$ Films as High-Performance Cathode Material in Quasi-Solid-State Thin-Film Lithium Batteries. *Applied Surface Science*, **657**; 159769

